Journal of Applied Polymer Science

Polysulfobetaine bearing tertiary amide between counterions and its applications

Vivek Arjunan Vasantha, Algin Oh Biying, Anbanandam Parthiban
Institute of Chemical and Engineering Sciences, Agency for Science, Technology and Research (A*STAR), 1, Pesek Road, Jurong Island 627833, Singapore
Correspondence to: V. A. Vasantha (E-mail: vivek_vasantha@ices.a-star.edu.sg) and A. Parthiban (E-mail: a_parthiban@ices.a-star.edu.sg)

ABSTRACT: Modified sulfobetaine bearing tertiary amide spacer between the counterions is synthesized and polymerized by reversible addition–fragmentation chain transfer polymerization technique. The tertiary amide spacer influences various characteristics of the zwitterionic polymer. The modified polyzwitterion, PZI, forms coacervates in deionized water. The coacervates are thoroughly characterized by scanning electron microscopy, transmission electron microscopy, and transmittance studies. The ability to form coacervate complexes with functional ingredients has been demonstrated by encapsulating renewable resource actives like ferulic acid. The coacervate complexes have been studied by optical microscopy, transmission electron microscopy, and automated sunscreen sun protection factor analyzer. Synergism is noticed in the coacervate complex. Because of its ability to form self-coacervates, this novel addition to the zwitterionic family is potentially useful for encapsulating many functional ingredients through coacervate complex formation. © 2017 Wiley Periodicals, Inc. J. Appl. Polym. Sci. **2017**, *135*, 46178.

KEYWORDS: applications; hydrophilic polymers; radical polymerization

Received 12 October 2017; accepted 10 December 2017
DOI: 10.1002/app.46178

INTRODUCTION

Zwitterionic polymers have been explored as a novel class of functional materials for many decades.[1–3] The interest in zwitterionic polymers surged ever since the report on its usefulness for antifouling applications[4] though recent trends point to its limited application scope in this regard.[5–7] Even before that zwitterionic polymers like carboxybetaines have been widely used as functional polymers for personal care applications in particular hair care applications for its effectiveness to control the texture of hair after washing thereby signifying the importance of this class of polymeric materials.[8–12] There are a wide variety of structurally diverse zwitterionic polymers with unique characteristics available now.[13–15] The introduction of newer entities into the chemical structure of zwitterionic polymers has resulted in polymeric materials with exceptional characteristics. This is predominantly due to enhanced inter polymer chain interactions caused by π-π interactions, π-cation interactions, and many others in addition to the existing charged interactions. These additional interactions dictate the conformation of polymer chains in aqueous medium. For example, enhanced π-π and donor-acceptor interactions influenced tremendously the critical salt concentration (CSC), that is, the minimum concentration of salt required to dissolve these polymers.[16] By introducing additional atoms like oxygen between counterions it was possible to further shift the salt concentration upward along with tremendous changes in nature of particles in dispersions even between adjacent homologues, that is, a difference of just one methylene unit.[17] In this series of modifications we hereby report the introduction of tertiary amide functionality between the counterions of sulfobetaine (Scheme 1). Unlike the oxygen atom introduced to make polysulfabetaines, the tertiary amide is well and truly a spacer separating the counterions because of its position between the counterions. This tertiary amide spacer offer two H-bond accepting sites and thus can be expected to further expand the properties of polysulfobetaine class of zwitterionic polymers. Unlike the conventional zwitterionic poly(acryl/methacryl amide)s where the amide is secondary in nature thus offering donor and acceptor H-bonding sites and also present as a pendant group farther from the zwitterions, the tertiary amide spacer presented here could make the zwitterions stiffer thereby inducing more interpolymer chain interactions.

In addition to the prevailing ionic interactions, the amide linkage can also be expected to induce self-assembly characteristics in solution. It may be noted that functionalities like tertiary amide have been used as a precursor for making polypeptide

Additional Supporting Information may be found in the online version of this article.

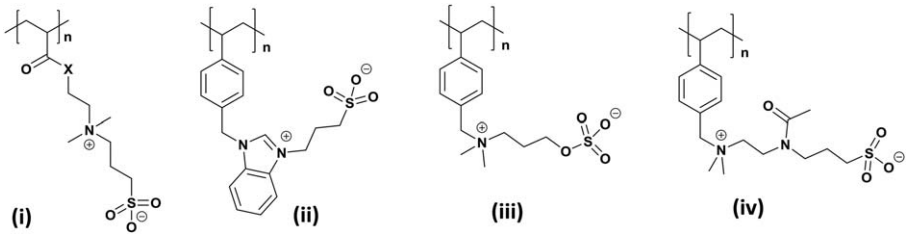

Scheme 1. Chemical structure of (i) conventional polysulfobetaines (X═O or ─NH), (ii) modified polysulfobetaine,[16] (iii) polysulfabetaines,[17] and (iv) polysulfobetaine of this work.

mimics because of its higher hydrolytic and conformational stabilities.[18] The self-assembly of natural and synthetic macromolecules is considered to be a robust strategy to construct novel functional materials. Coacervation is one such self-assembly process.[19] Charged polymers are capable of forming complex coacervates[20,21] and much progress has been made in the area of polyelectrolytes forming complex coacervates.[22,23] Reportedly chain architecture and stiffness of polymer chain play an important role in self-assembly driven coacervates.[24] Hence we also studied the coacervation behavior of tertiary amide spacer bearing polysulfobetaine. Thus this article provides details on the synthesis and characterization of novel polysulfobetaines that offer additional features like introduction of tertiary amide moiety between counterions. Detailed analysis of coacervate complexes formed by encapsulating bio-derived functional ingredients has also been provided.

EXPERIMENTAL

Materials

All reactions and polymerizations were performed with Schlenk technique under argon atmosphere. 1,3-Propanesultone (98%), 4,4′-azobis(4-cyanovaleric acid) (98.0%), 1,1,1,3,3,3-hexafluoro-2-propanol (99%), 2,2,2-trifluoroethanol (TFE, 99%), 2-methyl-2-oxazoline (98%), chlorobenzene (anhydrous, 99.8%), and trans-ferulic acid (FA, 99%) were purchased from Sigma-Aldrich (St. Louis, Missouri, USA) and used as received. The reversible addition–fragmentation chain transfer (RAFT) initiator 4-cyano-4-[(dodecylsulfanylthiocarbonyl) sulfanyl]pentanoic acid was purchased from Sigma-Aldrich. *N*-(4-vinylbenzyl)-*N*,*N*-dimethylamine was purchased from ACROS. The solvents such as acetonitrile (ACN) and *N*,*N*-dimethylformamide were freshly dispensed from Glass Contour–Solvent Purification System. All other solvents and chemicals used were of analytical grade obtained from Sigma-Aldrich and Merck. Microscopic quick read test (PMMA) slides were purchased from Globe Scientific. Ibidi flow cell chambers (μ-Slide I) were used to measure the stability of coacervates under the microscope. Deionized water used for swelling and other aqueous studies was purified by a Millipore water purification system with the resistivity of 18.0 MΩ cm.

Methods

3-(N-(2-(Dimethyl(4-Vinylbenzyl)Ammonio)Ethyl)Acetamido) Propane-1-Sulfonate (ZIM). The synthetic protocol for zwitterionic precursor 3-(2-methyl-4,5-dihydrooxazol-3-ium-3-yl)propane-1-sulfonate was as described previously[25,26] [Scheme 2(a)]. Briefly, in a 500 mL round bottom flask, 50 g (0.41 mol) of 1,3-propanesultone was dissolved in chlorobenzene (250 mL). 34.6 mL (0.41 mol) of 2-methyl-2-oxazoline dissolved in 50 mL of chlorobenzene was then added dropwise under argon atmosphere with stirring. The reaction mixture was heated at 50 °C for 24 h under the flow of argon gas. The solvent was removed under vacuum to obtain a colorless solid and washed with cyclohexane. The zwitterionic precursor was dried at 60 °C.

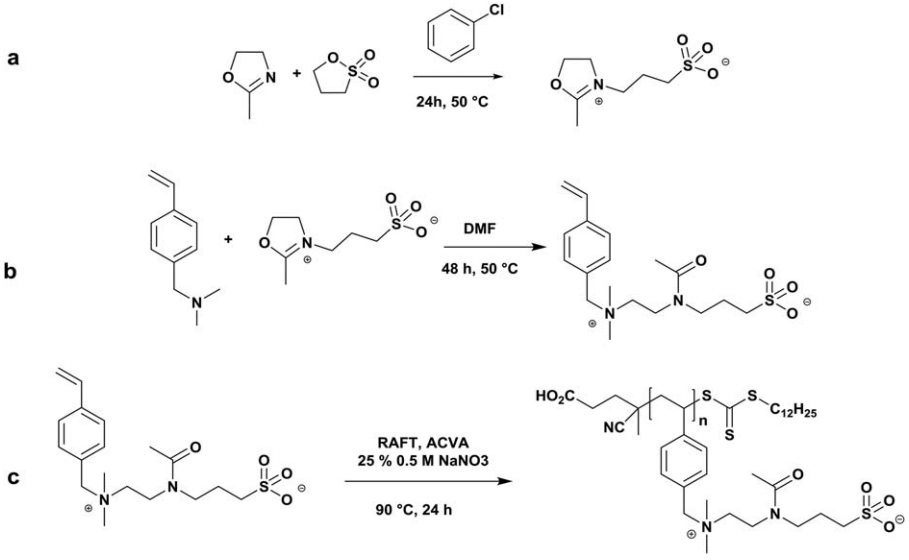

Scheme 2. Preparation of (a) zwitterionic adduct,[25,26] (b) zwitterionic monomer, and (c) polymer, PZI.

Yield = 71.3 g (84%). ^{1}H NMR (400 MHz, D2O, δ): 4.9 (t, 2H; —O—$\underline{CH_2}$), 4.2 (t, 2H; —N^+—$\underline{CH_2}$), 3.9 (t, 2 H; N^+—$\underline{CH_2}$—CH_2—CH_2—SO_3^-), 3.0 (t, 2H; $\underline{CH_2}$—SO_3^-), 2.47 (s, 3H; CH_3), 2.2–2 (m, 2H; CH_2); LC-TOF (ESI) *m/z*: $[M + H]^+$ calcd. for $C_7H_{13}NO_4S$, 207.06; found: 208.06.

In the second step, the ring opening of 3-(2-methyl-4,5-dihydrooxazol-3-ium-3-yl)propane-1-sulfonate using *N*,*N*-dimethylvinylbenzylamine to form desired zwitterionic monomer (ZIM) [Scheme 2(b)]. In a 250 mL round bottom flask, 21.8 g (0.105 mol) of 3-(2-methyl-4,5-dihydrooxazol-3-ium-3-yl)propane-1-sulfonate was dissolved in anhydrous *N*,*N*-dimethylformamide (200 mL). 27.2 mL (0.17 mol) of *N*,*N*-dimethylvinylbenzylamine was then added dropwise to the colorless solution. The reaction mixture was heated at 50 °C for 48 h. The solvent was removed and washed with acetone to obtain a colorless solid.

Yield = 28.9 g (74.5%). ^{1}H NMR (400 MHz, D2O, δ): 7.62–7.51 (m, 4H) CH_{aryl}; 6.7–6.8 (dd, 1H) $CH_{olefinic}$; 5.96 and 5.42 (d, 2H) $CH_{cis\ and\ trans}$; 4.5 (s, 2H) $CH_{2benzyl}$; 3.87 (t, 2H) N—$\underline{CH_2}$—CH_2—N; 3.44–3.53 (t, 4H) N—CH_2—$\underline{CH_2}$—N($COCH_3$) —$\underline{CH_2}$; 3.07 (s, 6H) $N(\underline{CH_3})_2$; 3.0 (t, 2H; $\underline{CH_2}$—SO_3^-)), 2.14 (s, 3H; $COCH_3$), 2.0–2.1 (m, 2H; —CH—$\underline{CH_2}$—CH_2—SO_3). LC-TOF (ESI) *m/z*: $[M + H]^+$ calcd. for $C_{18}H_{28}N_2O_4S$, 368.49; found: 369.18.

Polymerization of 3-(N-(2-(Dimethyl(4-Vinylbenzyl)Ammonio) Ethyl) Acetamido)Propane-1-Sulfonate, ZIM. In a dried Schlenk flask (100 mL), ZIM (5 g, 13.6 mmol), RAFT initiator (0.11 g, 0.27 mmol), 4,4′-azobis(4-cyanovaleric acid) (0.019 g, 0.068 mmol), and 0.5*M* $NaNO_3$ solution (25% w/v, 20 mL) was taken. The solution was purged with argon gas for 45 min. The reaction flask was degassed by three consecutive vacuum-argon sweeping cycles and sealed-off under the argon atmosphere at room temperature. Then the Schlenk flask was placed in a bath at 90 °C for 24 h. The resulting viscous solution was cooled and diluted with 5 mL of 0.5*M* $NaNO_3$ solution. The solution was then dialyzed against DI water for 3 days (MWCO = 1500) at 40 °C with repeatedly changing water. The resulting polymer was lyophilized and dried *in vacuo* at 50 °C.

^{1}H NMR (400 MHz, sat. NaCl/D_2O, δ): 7.6–6.9 (b, 4H) CH_{aryl}; 5.2 (b, 2H) $CH_{2benzyl}$; 4.3 (b, 2H) N—$\underline{CH_2}$—CH_2—N; 3.9–3.5 (b, 4H) N—CH_2—$\underline{CH_2}$—N($COCH_3$) —$\underline{CH_2}$; 3.4–3.1 (b, 6H) $N(\underline{CH_3})_2$ and (b, 2H) $\underline{CH_2}$—SO_3^-, 2.5–2.2 (b, 3H; $COC\underline{H_3}$) and (b, 2H) —CH—$\underline{CH_2}$—CH_2—SO_3; 1.9–1.3 (b, 3H) CH-CH_2. The molecular weights were confirmed by ^{1}H NMR and GPC: $M_{n,NMR}$ = 14,600 g/mol; [DP = ($I_{aromatic}$/4)/($I_{methyl(initiator)}$/3) and $M_{n,NMR}$ = DP × 368.49 + 403.67]; $M_{n,\ GPC}$ = 6300 g/mol (PDI 1.57); UV–vis (0.9 wt % NaCl): 224, 272, and 313 nm.

CHARACTERIZATION

The nuclear magnetic resonance (^{1}H NMR) spectra were recorded at room temperature on a Bruker UltraShield AVANCE 400SB spectrometer operating at 400 MHz. D_2O and 0.5, 0.9, 1.2 wt % and sat. NaCl/D_2O, respectively, were used as the solvent. The residual solvent peaks were used as internal standard. The aqueous GPC system was performed with a Delta 600 HPLC pump from Waters and was maintained at ambient temperature. 0.1*M* $NaNO_3$ in deionized water as eluent with the flow rate was 0.7 mL/min and the columns were maintained at 30 °C. The molecular weights were calculated by using poly (ethylene oxide) calibrations. Fourier transform infrared measurements were executed on a Digilab Excalibur FTIR Bio-Rad. The spectra were recorded in the range of 500–3500 cm^{-1} with the resolution of 4 cm^{-1}. The samples were either solvent cast on NaBr disc from 1,1,1,3,3,3-hexafluoro-2-propanol or as KBr pellets. High-resolution mass spectra were recorded using electrospray ionization (ESI) techniques in positive and negative ion modes by Thermo Finnigan MAT 95 XP. Mass spectral data is reported as the mass-to-charge ratio (*m/z*). UV absorption spectra were measured using a Shimadzu UV–vis UV 2700 spectrometer. The samples were measured in 1 cm cell path length and measured in the 200–600 nm regions. The scanning resolution was 2 nm. The surface tension measurements of aqueous PZI solution (freshly prepared) were performed by pendant drop method using OCA-50 Data Physics (Data Physics Instruments, Germany) at 25 °C. The droplet was equilibrated for 15 min in the controlled chamber. The hydrodynamic diameters and zeta potentials of PZI coacervates were evaluated by a Zetasizer Nano ZS dynamic light scattering (DLS) instrument (Malvern, UK) with Peltier heating system. The wavelength of 633 nm and the scattering angle of 173° were fixed at room temperature. The dispersant refractive index and the viscosity of aqueous NaCl were obtained from the database provided in the software.

Surface Characterization

Scanning Electron Microscopy. SEM images were recorded with JEOL JSM-6700F Field Emission. Images were observed with voltage acceleration of 5–10 kV. The lyophilized and dried samples were directly placed on aluminum stub using double-faced carbon tape and sputtering with gold before imaging.

Transmission Electron Microscopy. TEM images were collected on a Tecnai TF 20S-twin with Lorentz Lens Tec operated at 100–200 kV. Aliquots of coacervate samples were directly placed on the carbon coated grid, were used as received and allowed the solvent to evaporate. Encapsulated FA was dispersed in TFE (5 mg/mL), and 10 μL of the solution was used to cast. The casted samples were then left to dry on TEM grid at room temperature.

Optical Microscopy. The coacervates were placed on PMMA slides and imaged with the magnification of 10× and 40× using an optical microscope (Trinocular biological microscope TM Advance) with Toup View software. Image of coacervates were captured with an advanced 5.0 Mp camera under the control of software. Image analysis was performed with Toup view and ImageJ 1.51k software. Ibidi flow chambers (μ slide with adapter) were used to study the stability and reversibility of coacervates. The images were taken after 1 min after applied on the slides. The samples were observed separately for 30 to 60 min to study the coacervate stability. Typically 50 μL of PZI in aqueous salt (heated to 40 °C) placed on ibidi μ slide. As the temperature falls to room temperature, creating the diffusion of salt, results in PZI self-assembly. As the PZI approached coacervate micro droplets, reassembly occurred back to coacervate droplets on heating and cooling.

Automated Sunscreen SPF Analyzer. Solar light sunscreen protection factor (SPF) analyzer automated (SPF-290AS) was used to determine the critical wavelength, UVA/UVB, and Boot's star of PZI coacervates, ferulic acid, and PZI encapsulated ferulic acid. The transmitted light of UV radiation was measured from 290 to 400 nm at 1 nm interval on five different sites. The samples were prepared by micropipetting 100 mg at the concentration of 5% w/w—directly onto a quartz plate. The samples were smeared over the substrate and then left to dry inside a box for 30 min. WIN SPF software was used to determine critical wavelength, UVA/UVB ratio, and Boot's star results according to the FDA 2011 protocol (three references with five scans at different locations). The measurement was based on the amount of UV light passed through the sample compared to an uncoated substrate.[27,28]

Critical Wavelength (λ_c). The critical wavelength is the wavelength at which the sunscreen allows 10% of the rays to give broad-spectrum protection.[29–31] The ratio is calculated using the equation as follows:

$$0.9 \geq \frac{\int_{290}^{\lambda c} A\lambda d\lambda}{\int_{290}^{400} A\lambda d\lambda}$$

The critical wavelength is the value where 90% of the area of UV radiation is absorbed, reflected, or scattered of the absorbance spectrum from 290 to 400 nm. The critical wavelength above 370 nm, the level of protection is broad.

UVA/UVB ratio. The ratio of UVA to UVB was calculated by the software where a 1:3 ratio implies a broad spectrum protection.[29] UVA protection is determined by the UVA-PF test and UVB protection is determined as the SPF of a sunscreen. The general formula of UVA/UVB is as described below:

$$\text{UVA/UVB ratio} = \frac{\int_{320}^{400} A\lambda d\lambda}{\int_{290}^{320} A\lambda d\lambda}$$

Boot's Star System

Boot's star is a rating system between one and five stars that describes the ratio of UVA to UVB protection offered by sunscreen products.[29] One star indicates the low UVA protection while five stars indicate high UVA protection.

Preparation of PZI Coacervate Microdroplets. All coacervates were prepared in 4 mL clear glass vials at room temperature. PZI were measured as 0.05, 0.1, 0.26, 0.52, 1.01, 2.1, and 5% w/w, respectively, in DI water. The polymer solution was equilibrated at 25 °C for 18 h. The equilibrated solution was gently vortex for 30 s. The turbid suspension of liquid microdroplets was confirmed by the formation of coacervates from the optical microscope. Then, the same solutions were imaged using other microscopic techniques. For stability studies, 100 μL of the solution was applied to a slide for microscopy measurement. The slide was then allowed to stand at room temperature for 30–60 min.

For reversible coacervates, 1% w/w of PZI in 0.5% w/w of NaCl was prepared and titrated with DI water. The formation of turbid suspension from clear liquid results in the formations of the coacervate. The aqueous solution was heated at 60 °C and allowed to stand at room temperature result in reversible phase transition from clear to turbid and turbid to clear. The reversible turbid solution was visualized under the microscope.

For turbidity and surface tension measurements, the stock solution of 1% w/w of PZI was prepared using DI water. PZI added to DI water and allowed to stay overnight to hydrate for 18 h followed by gentle agitation with vortex mix for 30 s resulted in milky solution. The solution was further diluted to analyze the transmittance measurement.

Critical Coacervation Concentration or Coacervate Yield. From 0.05%–5% w/w PZI in DI water prepared as described earlier and gently vortex mixed for a few seconds after hydration overnight. The transmittance at 600 nm was used to evaluate the turbidity. $100 - \%T_{600}$ determined the phase transition (from clear to turbid) on increasing concentration of polymer. The transmittance was converted to turbidity, which was plotted against polymer concentration to give critical coacervation concentration. The increase in turbidity is associated with the coacervate formation. The optical image at higher concentration of PZI was observed for the onset of coacervation. The images were taken after the solution turned turbid.

Critical Salt Concentration. For the cloud point measurement, 1% w/w of PZI was prepared in 0.5% w/w NaCl. 1 mL of solution was titrated with DI water to determine CSC. On adding DI water to PZI aqueous salt solution, visually determined when the solution turned to cloudy. The phase transition on changing salt concentration was monitored using the transmittance at the wavelength of 600 nm. The transmittance was recorded on Shimadu UV–vis 570 spectrophotometer. The above obtained turbid solution was heated and cooled to visualize the reversible coacervates in the optical microscope.

Stability Studies. Transmittance analysis was performed using a Shimadzu UV–vis 570 spectrophotometer. The coacervate solution was taken in UV quartz tube. The transmittance was measured with respect to time using the kinetic method. Turbidity measurements were employed to investigate the characteristics of coacervation. DLS was used to study the temperature stability of the coacervates. The hydrodynamic diameters at different temperatures were measured and reported as the average of triplicate measurement.

Encapsulation Method. In a 4 mL clear glass vial equipped with magnetic stir bar, was added 1 mL of 1.0% w/w of PZI (10 mg) in 0.5% w/w NaCl solution. To this, FA (4.2 mg) was added. The solution was vigorously vortex mixed for 30 s. [10] μL of samples was observed under optical microscopy. The above solution was heated at 80 °C for 1 h. The turbid solution changed to clear solution. 10 μL of samples was observed under optical microscopy. The hot solution was transferred to the centrifuge tube (1.5 mL). The transparent solution was cooled to room temperature changes to turbid. FA was encapsulated through polymer phase-separated encapsulation. The encapsulated FA was centrifuged

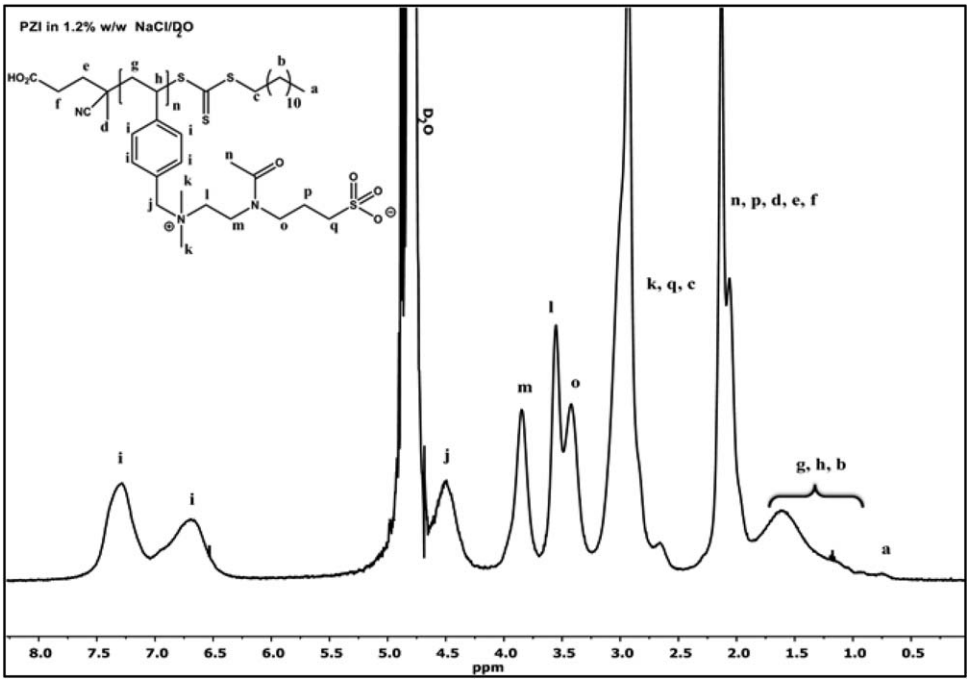

Figure 1. ^{1}H NMR of zwitterionic polymer PZI in D_2O/NaCl.

and washed with water and ethanol/water mixtures. The encapsulated FA was dried under vacuum. The dried encapsulated FA was dispersed in TFE and the size was measured using optical and TEM microscopes.

RESULTS AND DISCUSSION

Synthesis of Monomer and Polymer

The tertiary amide bearing ZIM was prepared in two steps as shown in Scheme 2. In the first step the adduct of oxazoline and 1,3-propanesultone was obtained by following a literature procedure.[17,18] The adduct was reacted with *N,N*-diemthyl-1-(4-vinylphenyl)methanamine to yield the modified ZIM. The modified sulfobetaine was then polymerized under RAFT mediated free radical polymerization. The ^{1}H-NMR spectra of precursors are shown in Supporting Information Figure S1 and that of polymer is shown in Figure 1. The molecular weight as determined by conventional techniques like gel permeation chromatography was lower than that determined by end group analysis using ^{1}H-NMR spectroscopy ($M_{n,\ \mathrm{GPC}} = 6300$ g/mol vs. $M_{n,\mathrm{NMR}} = 14{,}600$ g/mol) possibly due to difference in solution conformation with the standard used in GPC analysis.

Coacervation Behavior

PZI spontaneously self-assembled to liquid droplets on shaking gently with deionized (DI) water forming coacervates. Transmittance and light scattering studies were employed to determine the critical coacervation concentration. Figure 2 shows the transmittance results along with the appearance of PZI in water at varying concentrations. With increasing concentration of PZI in DI water the interfacial tension reduced as a result of charge build up at the interface. Figure 3 shows the variation in interfacial tension with concentration. Similarly, the particle size and size distribution as determined by DLS studies (Figure 4) with varying concentration also showed that the self-assembled particles were very intact at higher concentrations as indicated by the reducing size with increasing concentration until reaching a threshold after which the size remained more or less constant up to 5% w/w concentration (Supporting Information Figure S2).

Increasing PZI concentration influenced the particle size and particle size distribution. The average size of particles increased upon adding more of PZI at the initial stage. Coacervates formed with an intense surface activity that was able to absorb polymers at the expanding water/polymer interface leading to an increase in particle size. Thus the initial increase in size is due to the first complex formation and likely to be a microscopic phase transition. However, at higher concentrations, expansion of water/polymer interface lowered as more charged

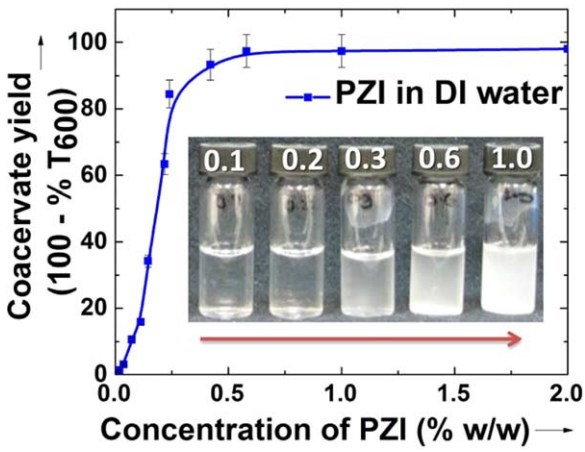

Figure 2. Transmittance with varying concentration of PZI (inset: formation of coacervates at different PZI (% w/w) concentrations. [Color figure can be viewed at wileyonlinelibrary.com]

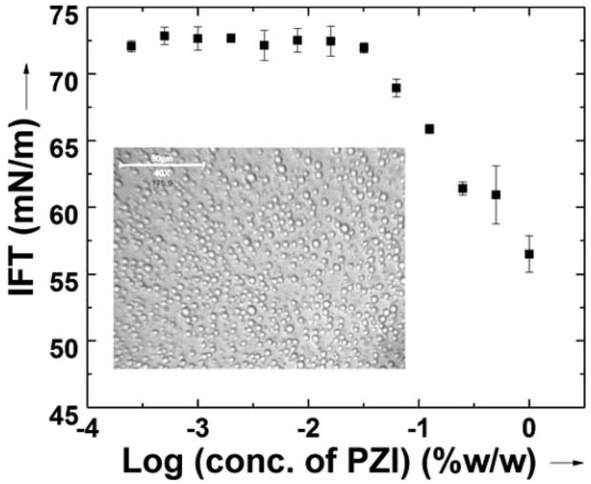

Figure 3. Change in interfacial tension with concentration of PZI in DI water (inset: optical microscopic image of 2% w/w PZI coacervates (scale: 50 μm).

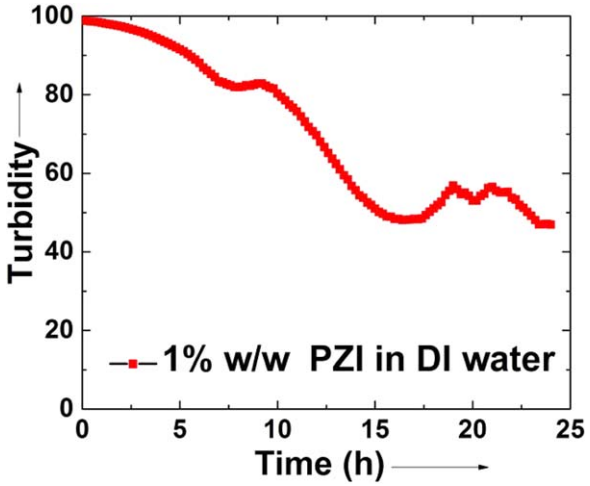

Figure 5. Stability of coacervates with time using 1% w/w PZI in DI water. [Color figure can be viewed at wileyonlinelibrary.com]

sites became available for interaction resulting in higher probability of complex formation. This in turn reduced the degree of hydration thereby leading to higher turbidity and therefore the coacervation yield. Upon further increasing the concentration of PZI, the microdroplets formed were more consistent in size and also the particle size did not change. This is beneficial in one way because the thicker wall formed can enhance the stability of encapsulated materials. The physically crosslinked PZI through zwitterionic interaction was stable against coalescence due to the zwitterionic stabilization and also the firm interaction between zwitterion and water through tertiary amide spacer. PZI helps to stabilize the dispersion and also helps in wall formation. Figures (3 and 4) (inset) and Supporting Information Figure S2 show the microscope images of self-coacervate droplets formed using PZI. The combined effects of ionic, nonionic, hydrophilic, and the polar spacer along with hydrophobic interactions are helpful to control the nature of dispersed microdroplets even when increasing the concentration of PZI.

The stability of coacervates was ensured by the ionic interactions and also the tertiary amide functionality may have helped to retain some voids thereby enabling retention of solvent. In the absence of such voids enforced by additional functionalities, the ionic interaction could become stronger resulting in more compact structures which could prevent the diffusion of water as is the case for layer by layer assembled surfaces using polyelectrolytes of opposite charges. The stability of coacervates with time and temperature are presented in Figure 5 and Supporting Information Figure S3. Also, the particle size more or less remained constant in the temperature range of 40 to 50 °C. In fact the size at 25 °C and 40–50 °C were similar except for about 30 °C. The spike in size noticed at 30 °C may be due to some phase changes occurring at this temperature similar to the sol–gel transition common in thermoresponsive polymers like polyacrylamides.

TEM image as shown in Figure 6 also indicated voided spherical particles of greater than 400 nm size with wall thickness of 90–200 nm for particles obtained from 0.6w/w % solution. It is useful to note that such voided structures are formed without

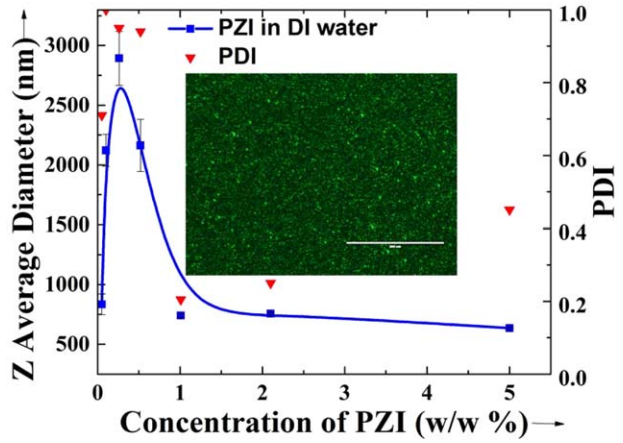

Figure 4. Particle size of PZI in DI water at different concentration [inset: PZI (2% w/w) coacervates under fluorescence microscope (scale bar: 200 μm)]. [Color figure can be viewed at wileyonlinelibrary.com]

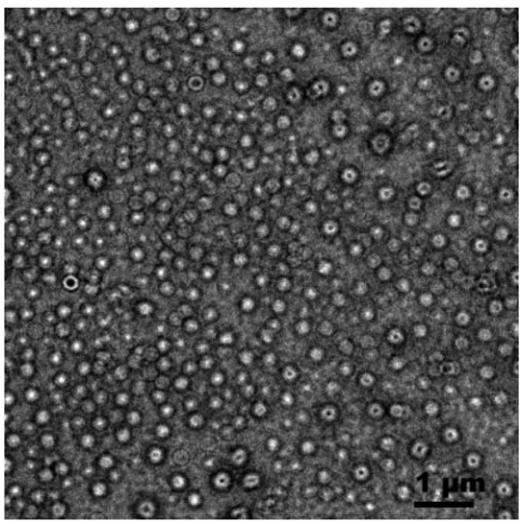

Figure 6. TEM micrographs of PZI coacervates in DI water (0.6% w/w) (scale bar: 1 μm).

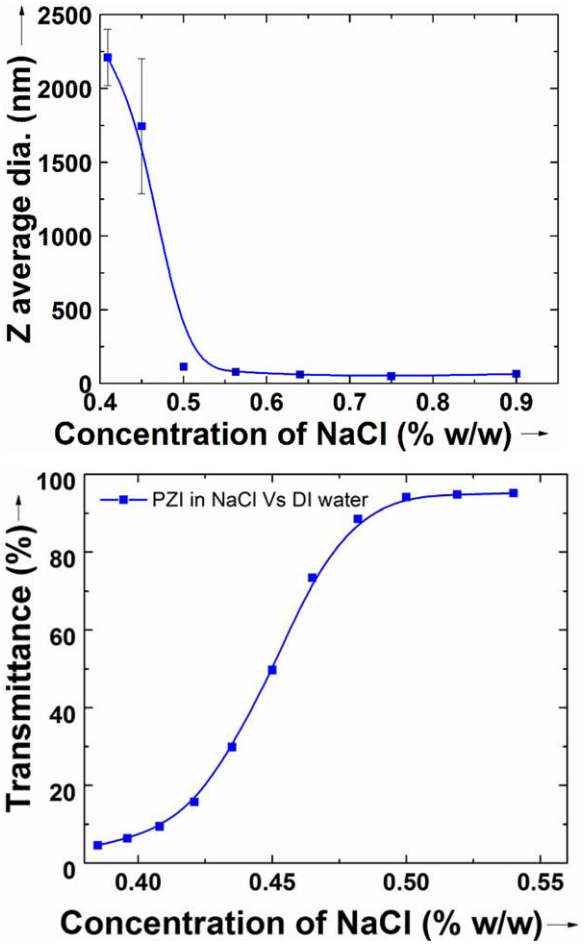

Figure 7. Effect of salt concentration on coacervate assembly as determined by DLS (a) and transmittance (b) studies. [Color figure can be viewed at wileyonlinelibrary.com]

the aid of any external agents or secondary processes as is commonly employed conventionally in the preparation of hollow spheres. Thermal treatment, acid etching, etc. are some of the common techniques used for making hollow spheres. Thus, for the first time, a synthetic polymer has shown, inherently, unique self-assembly behavior in water. It is worth noting that these hollow microcapsules are formed without the aid of any external agents. Hence such robust coacervates could be useful in some biomedical and consumer care applications.

Salt and Temperature Responsive Behavior

The assemblies of PZI in DI water could be disrupted by aqueous electrolyte solutions due to anti-polyelectrolyte behavior.[32–35] Cloud point titration studies were used to determine the minimum concentration of salt (CSC) needed to solubilize PZI. As shown in Figure 7 and also Supporting Information Figures S4–S7, CSC of 0.5% w/w of NaCl solution was required to completely break the self-assembled PZI. As expected, above this concentration PZI in water formed clear, transparent solution and below this concentration it was turbid. As the salt concentration or temperature increased (upper critical solution temperature), polymer chains were stretched with minimum or no intra- and interchain interactions. However, at lower salt concentration, turbid, phase-separated, coacervates formed rather than precipitation of polymer. This is in contrast to other polysulfobetaines. PZI presented here formed coacervates which are reversible and tunable. The role of spacer between zwitterionic groups in influencing the aqueous solution behavior is evident from ^{1}H-NMR and optical measurements as presented in various figures (Supporting Information Figures S4–S7).

Coacervation Complex

The low interfacial tension of PZI dispersion in DI water could be useful for forming coacervate complexes by encapsulating functional components. This was studied by encapsulating bio-derived active like ferulic acid. Ferulic acid is extracted from waste biomass such as rice and wheat bran and it is also present in various fruits. It has been proposed to possess many inherent beneficial characteristics.[36,37] However, because of its unstable nature, there have been many attempts to stabilize it. In this regard there are many reports which made ferulic acid as part of degradable polymer backbones so that it is released slowly.[38–41] Owing to the α,β-unsaturation prevailing in ferulic acid, it shows absorption maximum (λ_{max}) in the UV-B region thereby showing its potential as sunscreen compound. In a sense, ferulic acid is a derivative of cinnamic acid or rather 4-hydroxy cinnamic acid with an additional methoxy group *ortho*- to the phenolic group. 4-Methoxy ester derivatives of cinnamic acid are in use in cosmetic formulations as sunscreen for many decades. Therefore coacervate

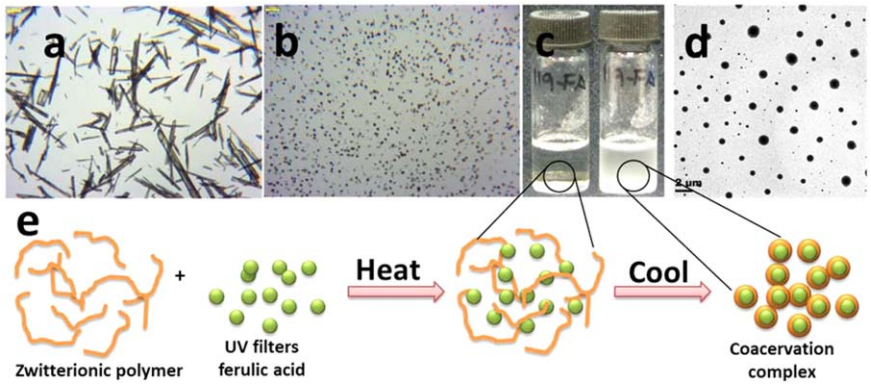

Figure 8. Optical microscopy of before (a) and after (b) encapsulation of ferulic acid using PZI (scale bar: 50 µm); The vials after encapsulation (c) TEM observation of encapsulated ferulic acid dispersed in TFE (scale bar: 2 µm), (high contrast is due to the high density of ferulic acid (d) and (e) graphic representation of encapsulation through coacervate complex. [Color figure can be viewed at wileyonlinelibrary.com]

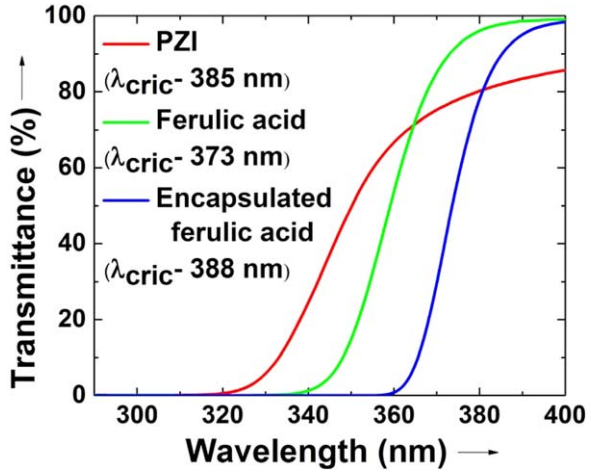

Figure 9. Diffused transmittance of PZI, ferulic acid, and the encapsulated coacervate complex. [Color figure can be viewed at wileyonlinelibrary.com]

complexes of ferulic acid with PZI bearing tertiary amide functionality in the ratio of 1:2 (w/w) were formed and characterized (Figure 8, Supporting Information Figures S8 and S9). The encapsulation efficiency was determined to be 72% (Supporting Information Table S1).

Figure 8 shows the optical microscopic image of ferulic acid before and after forming coacervate complex. Before coacervation, ferulic acid appeared as isolated and large bundles of needles or rods. The size of particles substantially reduced after complexation. This was further confirmed by TEM [Figure 8(d)] analysis which showed the retention of spherical morphology by the coacervate complex.

UV-Filter Performance

The transmittance studies of coacervate complex as well as that of PZI and ferulic acid showed that the coacervate complex possessed superior absorption characteristics. As compared to ferulic acid, the absorption of coacervate complex was red shifted by about 15 nm (Figure 9). The sunscreen characteristics of the coacervate complex and that of ferulic acid was determined by solar light (SPF) analyzer. The results of sun protection analysis are given in Table I. There is a trend toward making broad spectrum sunscreens, that is, the compounds are capable of absorbing in both UV-A and UV-B regions. Thus high ratios of UV-A/B are favorable. The UV-A/B ratio was higher for the coacervate complex than ferulic acid indicating the prevalence of some synergism in the coacervate complex. For an effective UV-A absorption, critical wavelength (λ_c) of above 370 nm is desirable. Both ferulic acid and the coacervate complex showed high λ_c with the coacervate complex showing even higher λ_c by about 15 nm.

Comparison between Polybetaines with and without Tertiary Amide Spacer

Polysulfobetaine synthesized with tertiary amide spacer showed unique solution behavior as compared with the polybetaine without amide spacer (Table II). In aqueous medium, PZI turned into translucent dispersion. In contrast, the polysulfabetaine formed a gel. This difference is likely due to the variation in degree of hydration along with the difference in ionic interactions introduced by the structural changes. Gel formation in polysulfabetaine without amide spacer is likely due to the prevalence of strong interchain interactions, whereas in the case of PZI, the tertiary amide may have introduced additional point of hydration. Also, the ease with which PZI disperses in aqueous medium points to the lessened interchain interactions. Indeed the interchain interactions in PZI are concentration dependent as can be noticed by the increasing coacervate size with increasing concentration. At higher temperatures, in the case of polysulfabetaine without amide spacer, the ionic interaction intensifies leading to the expulsion of hydrated water. This is indicated by the transition of translucent gel into turbidity caused by aggregation of polymer chains. On the contrary, coacervates of PZI remained stable at higher temperatures as well. This behavior of PZI is due to a combination of factors centered on the tertiary amide spacer. First and foremost, the tertiary amide group retained its ability to remain hydrated. Such hydrated tertiary amide group also kept the interchain interactions to the minimum thereby avoiding any aggregation.

The fact that the interaction between polymer chains, that is, interchain interactions through counterions in PZI is low can be further noticed in the CSC studies. In general, higher salt concentrations are required to break stronger ionic interactions in order to form fully solvated chains. The CSC (% w/w of NaCl) for PZI was 0.5 whereas that of polysulfabetaine without tertiary amide spacer was 8.4 clearly indicating the prevalence of far stronger ionic interactions in the absence of tertiary amide spacer.

CONCLUSIONS

The zwitterionic family of polysulfobetaine has been further expanded by adding a H-bond accepting functionality like tertiary amide between the counterions. The modified zwitterion formed coacervates in DI water. The ability of the modified polysulfobetaine to form coacervate complexes was demonstrated by encapsulating renewable functional component like ferulic acid. The encapsulation efficiency was high. The coacervate complex further enhanced the functional characteristics of ferulic acid. By considering the ease of preparation of polymers, this development opens up immense possibilities in the broad area of ionic polymers in particular zwitterionic polymers. The additional significance of these results may be noted by the

Table I. Results of Sunscreen Protection Factor Analysis

Samples	Critical wavelength (nm)	UVA/UVB	Boots rating	UVA protection
Ferulic acid (FA)	373	0.75	3	Good
Encapsulated FA	388	1.00	5	Maximum

Table II. Comparison between Zwitterionic Polymer with and without[17] Amide Spacer

Medium		With amide spacer 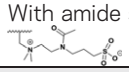	Without amide spacer[17] 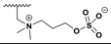
DI water	25 °C	Dispersion (coacervates)	Gel
	60 °C	Dispersion (coacervates)	Turbid
Critical salt concentration (CSC) (w/w % of NaCl)		0.45	8.4
Upper critical solution temperature	Above	Transparent	Transparent
	Below	Turbid with presence of coacervates	Turbid with aggregated particles
Salt and thermal responsive		Reversible coacervates	Precipitate

numerous opportunities that will open up when the tertiary amide functionality is subjected to other transformations. Similar to ferulic acid, it is also possible to form coacervate complex with many other functional ingredients.

ACKNOWLEDGMENTS

This work was funded by the Agency for Science, Technology and Research (A*STAR) of Singapore. The authors thank Zhao Wenguang (SEM), Heng Teck Huat (TEM), Noor Farhanah Binte Mohamed Barak (GPC), and Lewis Queh Yi Hong for interfacial tension analysis. We thank Samydurai Sudhagar, Genome Institute of Singapore, (A*STAR, Singapore) for fluorescence microscopic analysis.

REFERENCES

1. Ladenheim, H.; Morawetz, H. *J. Polym. Sci.* **1957**, *26*, 251.
2. Hart, R.; Timmerman, D. *J. Polym. Sci.* **1958**, *28*, 638.
3. Kudaibergenov, S.; Jaeger, W.; Laschewsky, A. In Supramolecular Polymers Polymeric Betains Oligomers; Donnio, B., Guillon, D., Harada, A., Hashidzume, A., Jaeger, W., Janowski, B., Kudaibergenov, S., Laschewsky, A., Njuguna, J., Pielichowski, J., Pielichowski, K., Takashima, Y., Eds.; Springer: Berlin, Germnay, **2006**; Vol. *201*, p 157.
4. Jiang, S.; Cao, Z. *Adv. Mater.* **2010**, *22*, 920.
5. Vasantha, V. A.; Jana, S.; Lee, S.-C.; Lim, C.-S.; Teo, S. L.-M.; Parthiban, A.; Vancso, J. G. *Polym. Chem.* **2015**, *6*, 599.
6. Yandi, W.; Mieszkin, S.; di Fino, A.; Martin-Tanchereau, P.; Callow, M. E.; Callow, J. A.; Tyson, L.; Clare, A. S.; Ederth, T. T. *Biofouling* **2016**, *32*, 609.
7. Vasantha, V. A.; Zainul Rahim, S. Z.; Jayaraman, S.; Junyuan, G. H.; Puniredd, S. R.; Ramakrishna, S.; Teo, S. L.-M.; Parthiban, A. *J. Mater. Chem. B* **2016**, *4*, 2731.
8. Boerwinkle, F. P.; Waxberg, D. L. (to 3M Center) U. S. Pat. 3,836,537 (**1974**).
9. Sterling, C. A. (to Minnesota Mining and Manufacturing Company). U. S. Pat. 4,075,131 (**1976**).
10. Langford, N. P.; Perrault, E. W. (to Minnesota Mining and Manufacturing Company). U. S. Pat. 4,066,589 (**1978**).
11. Yang, J. *Curr. Opin. Colloid Interface Sci.* **2002**, *7*, 276.
12. Somasundaran, P.; Purohit, P. *J. Cosmet. Sci.* **2011**, *62*, 251.
13. Laschewsky, A. *Polymer* **2014**, *6*, 1544.
14. Ilčíková, M.; Tkáč, J.; Kasák, P. *Polymer* **2015**, *7*, 2344.
15. Hildebrand, V.; Laschewsky, A.; Wischerhoff, E. *Polym. Chem.* **2016**, *7*, 731.
16. Vasantha, V. A.; Jana, S.; Parthiban, A.; Vancso, J. G. *Chem. Commun.* **2014**, *50*, 46.
17. Vasantha, V. A.; Jana, S.; Parthiban, A.; Vancso, J. G. *RSC Adv.* **2014**, *4*, 22596.
18. Priftis, D.; Tirrell, M. *Soft Matter* **2012**, *8*, 9396.
19. Bohidar, H. B. *J. Surf. Sci. Technol.* **2015**, *24*, 105.
20. Michaeli, I.; Overbeek, J. T. G.; Voorn, M. J. *J. Polym. Sci.* **1957**, *23*, 443.
21. Srivastava, S.; Tirrell, M. V. In Advances in Chemical Physics; John Wiley & Sons, Inc.: Hoboken, NJ, **2016**; p 499.
22. Perry, S.; Li, Y.; Priftis, D.; Leon, L.; Tirrell, M. *Polymer* **2014**, *6*, 1756.
23. Biesheuvel, P. M.; Cohen Stuart, M. A. *Langmuir* **2004**, *20*, 2785.
24. Lytle, T. K.; Radhakrishna, M.; Sing, C. E. *Macromolecules* **2016**, *49*, 9693.
25. Brunel, S.; Chevalier, Y.; Le Perchec, P. *Tetrahedron* **1989**, *45*, 3363.
26. Forestière, A.; Sillion, B. *J. Heterocycl. Chem.* **1980**, *17*, 1381.
27. Matts, P. J.; Alard, V.; Brown, M. W.; Ferrero, L.; Gers-Barlag, H.; Issachar, N.; Moyal, D.; Wolber, R. *Int. J. Cosmet. Sci.* **2010**, *32*, 35.
28. Moyal, D.; Galdi, A.; Oresajo, C. In Cosmetic Dermatology; Wiley-Blackwell: Hoboken, NJ, **2010**; p 144.
29. Springsteen, A.; Yurek, R.; Frazier, M.; Carr, K. F. *Anal. Chim. Acta* **1999**, *380*, 155.
30. Diffey, B. L. *Int. J. Cosmet. Sci.* **1994**, *16*, 47.
31. Diffey, B. L.; Tanner, P. R.; Matts, P. J.; Nash, J. F. *J. Am. Acad. Dermatol.* **2000**, *43*, 1024.
32. Schulz, D. N.; Peiffer, D. G.; Agarwal, P. K.; Larabee, J.; Kaladas, J. J.; Soni, L.; Handwerker, B.; Garner, R. T. *Polymer* **1986**, *27*, 1734.
33. Kumar, R.; Fredrickson, G. H. *J. Chem. Phys.* **2009**, *131*, 104901.
34. Kumar, N.; Pruthi, V. *Biotechnol. Rep.* **2014**, *4*, 86.

35. Delgado, J. D.; Schlenoff, J. B. *Macromolecules* **2017**, *50*, 4454.
36. Maurya, D. K.; Devasagayam, T. P. A. *Food Chem. Toxicol.* **2010**, *48*, 3369.
37. Srinivasan, M.; Sudheer, A. R.; Menon, V. P. *J. Clin. Biochem. Nutr.* **2007**, *40*, 92.
38. Ouimet, M. A.; Faig, J. J.; Yu, W. L.; Uhrich, K. E. *Biomacromolecules* **2015**, *16*, 2911.
39. Ouimet, M. A.; Griffin, J.; Carbone-Howell, A. L.; Wu, W.-H.; Stebbins, N. D.; Di, R.; Uhrich, K. E. *Biomacromolecules* **2013**, *14*, 854.
40. Noel, A.; Borguet, Y. P.; Raymond, J. E.; Wooley, K. L. *Macromolecules* **2014**, *47*, 2974.
41. Beristain, M. F.; Nakamura, M.; Nagai, K.; Ogaw, T. *Des. Monomers Polym.* **2009**, *12*, 257.